Progress In Electromagnetics Research B, Vol. 60, 63–77, 2014

HRR Profiles Time-Frequency Non-Negative Sparse Coding for SAR Target Classification

Xinzheng Zhang[1, *], Qizheng Wu[1], Shujun Liu[1], Jianhong Qin[1], and Wei Song[2]

Abstract—A new approach to classify synthetic aperture radar (SAR) targets is presented based on high range resolution (HRR) profiles time-frequency matrix non-negative sparse coding (NNSC). Firstly, SAR target images have been converted into HRR profiles. And the non-negative time-frequency matrix for each of the profiles is obtained by using an adaptive Gaussian representation (AGR). Secondly, NNSC is applied to learn target time-frequency basis of the training set. Feature vectors are constructed by projecting each HRR profile time-frequency matrix to low dimensional time-frequency basis space. Finally, the target classification decision is found with support vector machine and nearest neighbor algorithm respectively. To demonstrate the performance of the proposed approach, experiments are performed with Moving and Stationary Target Acquisition and Recognition (MSTAR) public release SAR database. The experimental results support the effectiveness of the proposed technique for SAR target classification.

1. INTRODUCTION

Synthetic aperture radar (SAR) is a coherent radar system which has the ability to produce high-resolution remote sensing images in all-weather condition [1]. In order to achieve high cross-range resolution, SAR collects data from multiple observation points, and focuses the echo coherently to obtain a two-dimensional high-resolution description of the scene. Automatic Target Recognition (ATR) systems using SAR sensors have been the subject of research in the area of military defense for many years [2]. Due to the unique characteristics of SAR image formation process, such as specular reflection, multiple bounces and nonliteral natures of the data, it is difficult to extract effective features for ATR as used in optical image. It is important to develop efficient and robust feature extraction and classification algorithms for ATR systems [3].

There is a broad class of feature extraction method based on two-dimensional SAR images for target classification. The most straightforward approach is to use a SAR target image's intensity values to directly generate image features [4, 5]. Another popular approach feature extraction technique is based on wavelet transform or multi-scale approach [6]. Alternatively, the features such as target region outline descriptors or ridges can also be extracted to classify targets [7, 8]. Physics-based features can be extracted using scattering center models, which provide a concise, physically relevant description of the target [9]. There are also several target features extraction methods based on shadow regions in a SAR image [10].

However, SAR target classification can also use features extracted from high resolution range (HRR) profiles converted from a SAR complex image [11]. Compared to image-based feature extraction techniques, one benefit of HRR profiles feature extractions for SAR ATR is the ability to exploit target-sensor aspect dependent scattering characteristics. In addition, it is also prior to image-based feature extraction when SAR images are blurred or low-SNR due to target moving or other factors [12]. Some

Received 4 April 2014, Accepted 16 May 2014, Scheduled 26 May 2014

* Corresponding author: Xinzheng Zhang (zhangxinzheng03@126.com).

[1] College of Communication Engineering, Chongqing University, Chongqing 400044, China. [2] School of Information Engineering, Minzu University of China, Beijing 100081, China.

researchers have proposed a number of recognition features based on SAR target HRR profiles. Power spectrum features of HRR profiles are employed for SAR target recognition [13]. One-dimensional scattering centers of HRR profiles are investigated for target recognition via Relax algorithm [11]. SAR target classification is also researched from HRR profiles high order statistic features [14]. From these works, it can be seen that how to extract robust and effective features of HRR profiles is very important in the HRR profiles-based SAR target recognition.

In terms of radar target HRR profiles feature extraction, it has been found that exploitation of time-frequency (T-F) domain features can be effective for target detection and discrimination. T-F analysis techniques have long been used to reveal the complicated scattering mechanisms concealed in radar echoes [15]. In [16], T-F geometrical moments features extraction method is derived for radar target classification. An approach is developed using T-F analysis for human gait radar signals [17]. T-F analysis techniques are also successfully applied to exploit radar target micro-Doppler signature as shown in [18]. When using time-frequency features for radar target recognition, the most critical issue is to recover discriminative information while reducing the dimension of the time-frequency plane data. Our focus in this paper concentrates on developing a new feature extraction technique in T-F domain based on non-negative sparse coding (NNSC). Sparse coding is an efficient way of coding information, in which most of the code elements are zero and not active [19, 20]. It is well known that sparse coding has succeeded in areas including image processing and pattern recognition [21, 22]. In conventional sparse coding, the data are described as a combination of elementary features which include both additive and subtractive components. However, the fact that features can 'cancel each other out' using subtraction is contrary to the intuitive notion of combining parts to form a whole. Thus, completely non-negative sparse coding have been investigated in [23]. Recently, NNSC has emerged as a useful feature extraction method in areas related to face recognition and image denoising [24, 25]. In this work, non-negative T-F representations has been applied to target HRR profiles to obtain non-negative T-F data matrix, so NNSC is naturally considered for non-negative T-F feature extraction. This paper investigates how NNSC is applied to learn features of HRR profiles T-F matrix and can be used for SAR target classification.

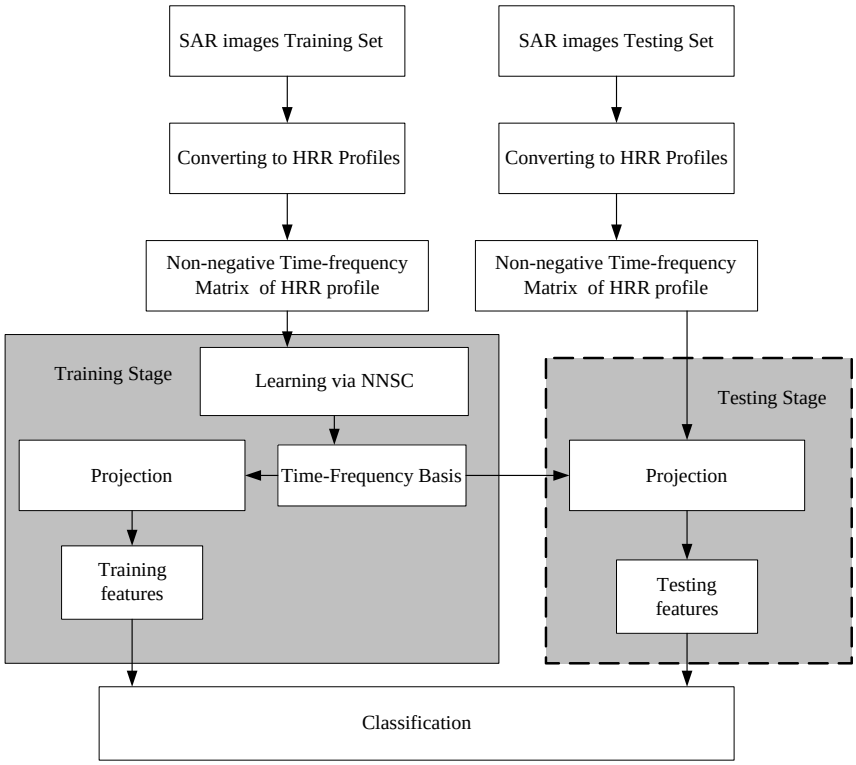

Figure 1. The procedure of the proposed SAR target classification approach.

Figure 1 highlights the contribution of this paper in the developed SAR target classification procedure. To fulfill the above objectives, in the first point, target HRR profiles are converted from each corresponding SAR complex image. In the second point, we choose the T-F analysis tool of adaptive Gaussian representative (AGR) to obtain each HRR profile non-negative T-F matrix. In the third stage of this paper, NNSC is used to learning T-F basis based on training data set and extract time-frequency features for both training and testing data sets. In the last stage, experiments are carried out on MSTAR public release database in order to evaluate the effectiveness of the proposed approach.

The rest of this paper is organized as follows. In Section 2, the method of HRR profiles converted from SAR image is described, and non-negative T-F analysis of HRR profile is investigated utilizing adaptive Gaussian representation (AGR). In Section 3, the theory of NNSC is reviewed briefly. Section 4 presents the principles of applying NNSC to SAR target classification. The experimental verification of the proposed approach using Moving and Stationary Target Acquisition and Recognition (MSTAR) public release database is presented in detail in Section 5. Finally, the conclusions are summarized in Section 6.

2. SAR TARGET HRR PROFILE *T*-*F* ANALYSIS

2.1. Conversion from SAR Complex Image to HRR Profiles

As discussed above, a SAR target image has to be converted into HRR profiles. Because we use the MSTAR public release SAR dataset considered for the experiments in this work, we briefly describe the procedure of how MSTAR SAR image chips are converted to HRR profiles which is detailed in [11].

Consider a SAR complex image $\mathbf{S}(d, c)$, where d reflects the downrange dimension and c the cross range. A two-dimensional (2D) inverse FFT is taken of $\mathbf{S}(d, c)$ to obtain the corresponding phase history data. Next, the deconvolution of the weighting and removal of the zero-padding is performed for the phase history data due to the operation of Taylor window weighting and zero-padding in SAR image formation.

Then, a 2D FFT is applied to produce a deconvoluted and Nyquist-sampled image $\mathbf{S}'(d, c)$. Note that both the target and surrounding clutter exist in $\mathbf{S}'(d, c)$. So, to remove the clutter, a target segmentation procedure is taken to the image $\mathbf{S}'(d, c)$. Then, an inverse FFT is performed in the cross dimension for all d, of which each d-dependent waveform, for a fixed c, corresponds to a HRRP. At last, for MSTAR SAR data, each 128×128 SAR complex image can obtain 100 HRR profiles. Figure 2 depicts an example of the conversion of one BMP2 targets SAR image.

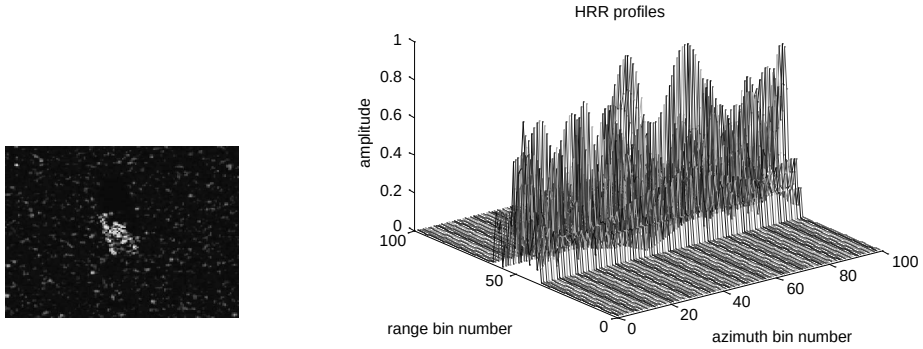

Figure 2. An example of conversion from a SAR complex image to HRR profiles. (a) BMP2 target SAR image. (b) HRR profiles.

2.2. HRR Profile Time-frequency Analysis Based on AGR

T-F domain indicates a two-dimensional energy representations of a signal in terms of time and frequency domains. There are several T-F approaches, such as the short-time Fourier transform (STFT),

Wigner-Ville distribution (WVD), adaptive Gaussian representation (AGR). However, not all the T-F analysis methods are suitable for radar HRR profiles feature extraction purposes. In this study, we select AGR to represent HRR profiles in the T-F domain. Compared to other T-F approaches, AGR can decompose the radar signal into T-F centers corresponding to scattering centers and local resonances with high T-F resolutions. AGR can give a joint T-F distribution which is non-negative, adaptive and cross-term interference free. The advantage of AGR processing for radar applications has been well described in [14, 15]. Up to now, AGR has been successfully applied in ISAR imaging, complicated scattering diagnostic, and radar target classification.

AGR expands a HRR profile in time-domain $r(t)$ in terms of normalized Gaussian elementary functions $g_i(t)$ with an adjustable T-F center $(t_i,\ f_i)$ and a variance α_i

$$r(t) = \sum_{i=0}^{\infty} C_i g_i(t). \tag{1}$$

where

$$g_i(t) = \left(\frac{1}{\pi\alpha_i}\right)^{\frac{1}{4}} \exp\left\{-\frac{(t-t_i)^2}{2\alpha_i}\right\} \cdot \exp\left(j2\pi f_i t\right).$$

The adjustable parameters t_i, f_i and α_i for Gaussian basis functions, and C_i for the coefficient can be obtained such that $g_i(t)$ is most similar to $r_i(t)$.

$$|C_i|^2 = \max_{t_i,f_i,\alpha_i} \left| \int r_i(t) g_i^*(t) dt \right|^2, \quad \alpha_i \in R^+, \quad t_i, f_i \in R. \tag{2}$$

where $r_i(t)$ is the remainder after the orthogonal projection of $r_{i-1}(t)$ onto $g_{i-1}(t)$, and this iterative procedure is described as

$$r_i(t) = r_{i-1}(t) - C_{i-1} g_{i-1}(t) \tag{3}$$

Since the projection integral in (2) is the Fourier transform of $r_i(t)$ with the Gaussian window $u(t) = (\pi\alpha_i)^{-0.25} \exp[-((t-t_i)^2/2\alpha_i)]$, the adjustable T-F center $(t_i,\ f_i)$ and associated variance α_i can be obtained using FFT and the specific search procedure in [6]. The t_i, f_i, α_i, and C_i finally obtained give the solution of (2) and these four parameters completely describe one Gaussian T-F basis function at the i-th iteration.

After $i_{\max}$ stages of AGR decomposition, the following relationships hold

$$r(t) = \sum_{i=0}^{i_{\max}} C_i g_i(t) + r_{i_{\max}+1}(t). \tag{4}$$

And

$$\|r(t)\|^2 = \sum_{i=0}^{i_{\max}} |C_i|^2 + \|r_{i_{\max}+1}(t)\|^2 \tag{5}$$

Therefore, the AGR iteration in (3) continues until the reconstruction error $\|r_{i_{\max}+1}(t)\|^2$ is sufficiently small, hence, the upper limit $i_{\max}$ is determined.

After t_i, f_i, α_i, and C_i, $i = 0, 1, 2, \ldots, i_{\max}$ are obtained via AGR processing, the T-F matrix, which represents a signal energy distribution in the joint T-F plane, and $\Theta(t, f)$ is given by

$$\Theta(t,f) = \sum_{i=0}^{i_{\max}} 2\,|C_i|^2 \exp\left\{-\frac{(t-t_i)^2}{2\alpha_i} - (2\pi)^2\alpha_i(f-f_i)^2\right\}. \tag{6}$$

In Figure 3, T-F matrices of several HRRPs from BMP2 target and BTR70 target using AGR technique are depicted. In this work, each T-F matrix has a size of 100 by 100 for a HRR profile with 100 sampling points. It can be seen that all T-F matrices are sparse and localization.

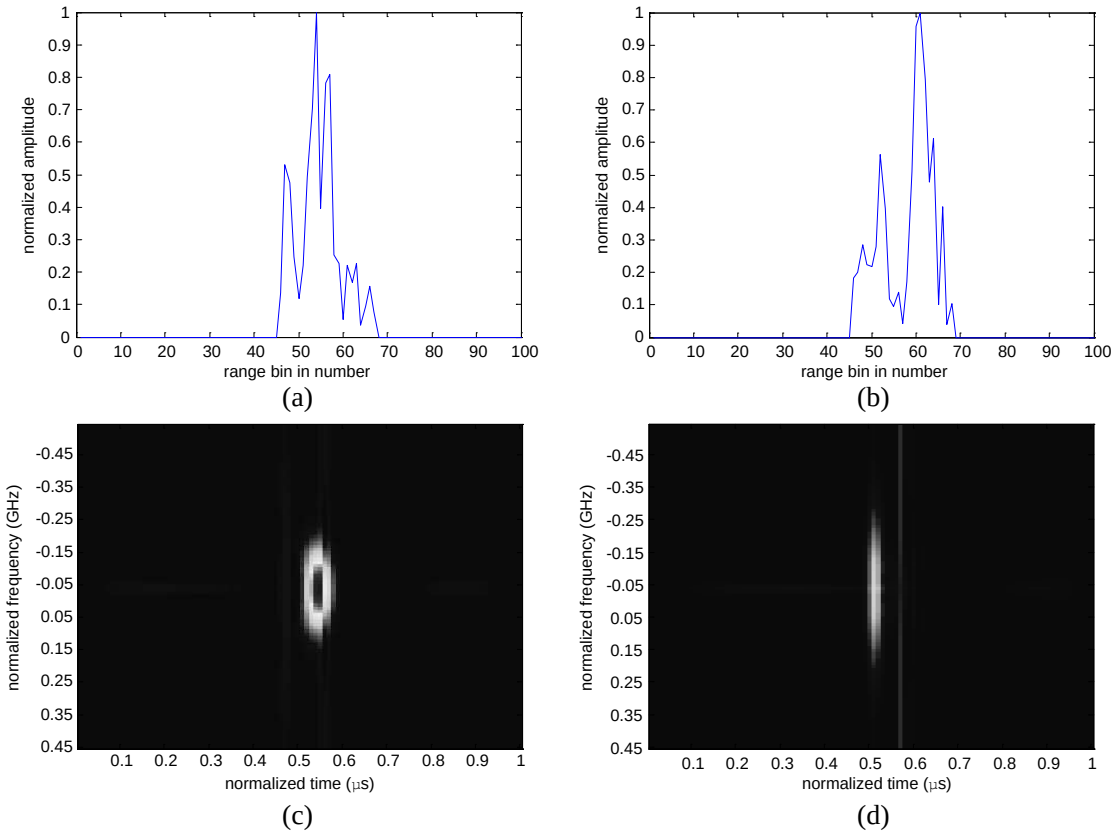

Figure 3. T-F matrices of several HRRPs from different targets, (a) a HRRP of BMP2 target, (b) a HRRP of BTR70 target, (c) T-F matrix of the HRRP in (a), (d) T-F matrix of the HRRP in (b).

3. NON-NEGATIVE SPARSE CODING

NNSC is an adaptive representation of the statistics of the data and has its roots in neural information processing, which is proposed in [22]. It is argued that when NNSC model is learnt from image data, the learnt basis components have the properties of the spatial receptive fields of simple cells in the primary visual cortex [26]. So, the NNSC technique provides a principled method for using training data to determine the significant parts of an image, which has been successfully applied in image denoising and pattern recognition. In this paper, as a T-F matrix of a HRR profile is non-negative, it can be treated and processed as an image.

The basic idea behind NNSC is as follows. An observed multi-dimensional non-negative vector $\mathbf{z}$ is modeled as a linear combination of a number of non-negative basis vectors represented by $\mathbf{D} = [\mathbf{D}_1, \ldots, \mathbf{D}_k]$. That is, let an image $\mathbf{z}$ with n non-negative pixel be represented by

$$\mathbf{z} = \mathbf{D}\mathbf{h} = \sum_{k=1}^{K} \mathbf{D}_k \mathbf{h}_k \tag{7}$$

The K columns of $\mathbf{D}$ are the bases images, and each of them is an n dimensional vector. Thus, $\mathbf{D}$ is an $n \times K$ matrix. The K-dimensional non-negative coefficient vector $\mathbf{h}$ provides specific contribution of each basis vector. The crucial assumption in the NNSC technique is that the coefficient vector exhibits sparseness. The goal is to select a set of basis, so that $\mathbf{z}$ can be represented sparsely and accurately. It has been shown that imposing non-negativity constraints leads to a part-based representation, because only additive and not subtractive combinations are allowed. The enforcing sparsity of the coefficient vector leads to solutions where only a few bases are active simultaneously. This can lead to better solutions, because it forces the basis to be more source specific.

For T-F matrices feature extraction in this paper, Equation (7) is extended from representing a single T-F matrix to a set of T-F matrices. Let a dataset of m training T-F matrices be given as an $n \times m$ matrix $\mathbf{Z}$ with each column consisting of n non-negative pixel values of a T-F matrix. This matrix $\mathbf{Z}$ is approximately factorized into the $n \times K$ basis matrix $\mathbf{D}$ and an $K \times m$ matrix $\mathbf{H}$. Each T-F matrix can then be represented as a linear combination of the basis matrices using the approximate factorization:

$$\mathbf{Z} \approx \mathbf{DH} \tag{8}$$

where $\mathbf{D}$ and $\mathbf{H}$ are non-negative matrices which is referred to as the dictionary and the sparse code. The columns of the dictionary matrix constitute a source specific basis, and the sparse code matrix contains weights. Each column of $\mathbf{H}$ contains the weights needed to approximate the corresponding columns in $\mathbf{Z}$ using the bases from $\mathbf{D}$.

Combining the goal of small reconstruction error with that of sparseness, the following objective function to be minimized can be arrived [5].

$$\Omega_{\mathrm{NNSC}}(\mathbf{D}, \mathbf{H}) = \sum_{i=1}^{n} \sum_{j=1}^{m} \left(\mathbf{Z}_{ij} - \sum_{l=1}^{K} \mathbf{D}_{il} \mathbf{H}_{lj} \right)^2 + \lambda \sum_{k=1}^{K} \sum_{j=1}^{m} \xi(\mathbf{H}_{kj}) \tag{9}$$

Subject to the constraints $\forall i, j, k, l : D_{il} \geq 0$, $H_{lj} \geq 0$, and $|d_j| = 1$, where d_j denotes the jth column of $\mathbf{D}$. The sparseness parameter λ is a constant that controls the tradeoff between accurate reconstruction and sparseness. When λ equals zero, the objective function reduces to the squared error version of non-negative matrix factorization (NMF) [25]. The form of ξ defines how sparseness is measured, and it is suggested that a typical choice for ξ is $\xi(H_{kj}) = |H_{kj}|$ in [11].

The NNSC learning algorithm includes two parameters, the sparseness factor $\lambda \geq 0$ and the iterative step size μ for the projected gradient descent. The objective function is non-increasing under the following update rules [23]:

$$\mathbf{H}_{kj} \leftarrow \mathbf{H}_{kj} \sum_{i=1}^{n} \frac{\left[\mathbf{D}^T \mathbf{Z}\right]_{kj}}{[\mathbf{D}^T \mathbf{DH}]_{kj} + \lambda} \tag{10}$$

$$\mathbf{D} \leftarrow \mathbf{D}^T - \mu \left(\mathbf{D}^T \mathbf{H} - \mathbf{Z}\right) \mathbf{H}^T \tag{11}$$

$$\mathbf{D}_{kl} \leftarrow \frac{\mathbf{D}_{kl}}{\sum_{k=1}^{n} \mathbf{D}_{kl}} \tag{12}$$

where $[\,]_{kj}$ indicates that the noted divisions and multiplications are computed element by element. This projected gradient decent step is guaranteed to decrease the objective function if the step size $\mu \geq 0$ is small enough. However, there is no guarantee of reaching the global minimum, due to the non-convex constraints:

$$\Omega_{\mathrm{NNSC}}\left(\mathbf{D}^{(t+1)}, \mathbf{H}^{(t+1)}\right) \leq \Omega_{\mathrm{NNSC}}\left(\mathbf{D}^{(t)}, \mathbf{H}^{(t)}\right); \quad t \geq 0 \tag{13}$$

4. SAR TARGET CLASSIFICATION USING NNSC

4.1. NNSC Features Extraction

The task of SAR target classification using NNSC is depicted in Figure 1, which mainly includes two stages. One stage is training in which the training SAR target NNSC features are extracted for later use. At another stage of testing, each test input is presented to the system sequentially, and testing NNSC features are extracted. The target type is found by performing classification algorithm with support vector machine (SVM) or nearest neighbor (NN) decision.

In this paper, although a SAR target image can be converted into 100 HRR profiles, we extract one from every 10 HRR profiles for the following feature extraction on the consideration of computation cost reduction. So, there are 10 T-F matrices for each SAR target image. For an individual HRR T-F

matrix $\mathbf{z}_i^p$ ($i = 1, \ldots, 10$) of a training SAR image from the target p, the corresponding feature vector $\mathbf{v}_i^p$ is obtained by projecting $\mathbf{z}_i^p$ to lower dimensional basis feature space as follows.

$$\mathbf{v}_i^p = \left(\mathbf{D}^T\mathbf{D}\right)^{-1}\mathbf{D}^T\mathbf{z}_i^p \tag{14}$$

The feature vector $\mathbf{v}^p$ of a training SAR image from the target p can be constructed in sequence by $\mathbf{v}_i^p$ as follows:

$$\mathbf{v}^p = [\mathbf{v}_1^p, \ldots, \mathbf{v}_{10}^p] \tag{15}$$

A similar way as above is applied to extract testing feature vectors $\mathbf{v}^q$.

4.2. Classification Algorithm

For comparison, in later experiments, SVM and NN algorithms are applied respectively in the classification stage.

4.2.1. NN Classification Algorithm

In NN classification algorithm, the distance $\eta(\mathbf{v}^q, \mathbf{v}^p)$ is computed between the testing feature vector and the training feature vector. The target type is classified as the class to which the closest training feature vector belongs. For the experiments carried out in this paper, classification is decided using Euclidean distance as follows.

$$\eta\left(\mathbf{v}^q, \mathbf{v}^p\right) = \left\|\mathbf{v}^q - \mathbf{v}^p\right\|_2^2 \tag{16}$$

where $\|\cdot\|_2^2$ means l_2-norm.

4.2.2. SVM

SVM classifiers are based on the principle of structural risk minimization [5]. Assuming a set of N training samples and labels $\{\mathbf{v}_i, y_i\}_{i=1,\ldots,N}$, the result of training the SVM is the hyperplane decision function

$$\varepsilon(\mathbf{v}, \alpha) = \sum_{i=1}^{N} \alpha_i y_i \phi(\mathbf{v}_i, \mathbf{v}) + b \tag{17}$$

where, variables α_i are Lagrange multipliers. $\phi(\mathbf{v}_i, \mathbf{v})$ is the kernel function of the test feature vector with the training feature vectors and b the bias from the feature space origin. The classification of the test data is based on the sign of the decision function indicating which side of the hyperplane the pattern falls on in the feature space. Here, for $\phi(\mathbf{v}_i, \mathbf{v})$ we choose the radial basis kernel function as follows.

$$\phi\left(\mathbf{v}_i, \mathbf{v}\right) = \exp\left(-\frac{\left\|\mathbf{v}_i - \mathbf{v}\right\|^2}{2\sigma^2}\right) \tag{18}$$

where, σ is the kernel width parameter.

The SVM classifier is initially a binary classifier. Therefore, some methods are needed to extend SVM in a multi-class problem. To achieve this, one simple but valuable method is based on combining binary classification results with a proper consensual rule such as majority voting. In the literature, there are two techniques widely used. They are One-Against-All (OAA) strategy and One-Against-One (OAO) strategy. In the literature, OAO strategy takes more computational time than OAA Strategy that has been reported [27]. Additionally, more classification accuracies are usually obtained by using OAA strategy. Therefore, OAA strategy is chosen in this paper to get highest results obtained by SVM classifiers.

5. EXPERIMENTAL RESULTS

5.1. Database

In this paper, we use the Moving and Stationary Target Acquisition and Recognition (MSTAR) public release database to evaluate the SAR target classification performance of the proposed approach. This is a standard dataset for SAR ATR algorithm, consisting of X-band SAR images for ten targets [28]. These targets include BMP2 (tank), BRDM2 (truck), BTR60 (armored car), BTR70 (armored car), D7 (bulldozer), T62 (tank), T72 (tank), ZIL131 (truck), ZSU234 (cannon), 2S1 (cannon). Visible light images of these targets are shown in Figure 4. Examples of MSTAR SAR images at near aspect angles are shown in Figure 5. Each image has a size around 128 by 128. Different target images may have slightly different sizes. The images are already centered with 0 to 360 degree of orientation. Since all the targets have similar length and width, the size and shape of target images at near aspect angles are almost the same, which makes the traditional feature extraction methods ineffective for this application. Unlike optical images, a SAR image reflects the structure of target's scatters, which does not have even reflect rate over different angles. Thus SAR images of the same target taken at different orientation angles can show great difference, which makes classification even more difficult. For each target, images

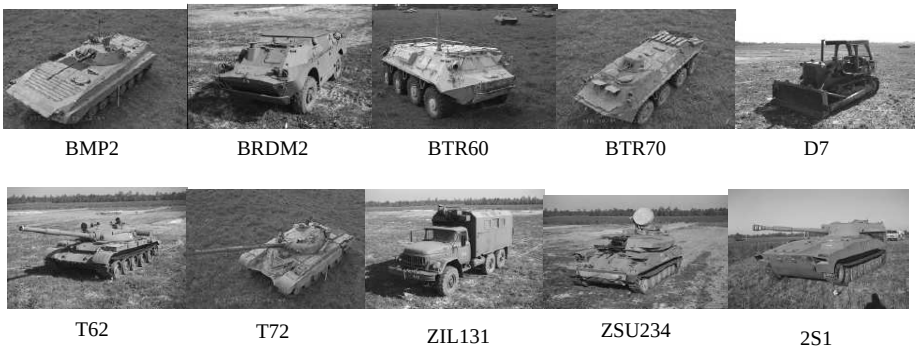

Figure 4. Visible light images of ten targets in MSTAR database.

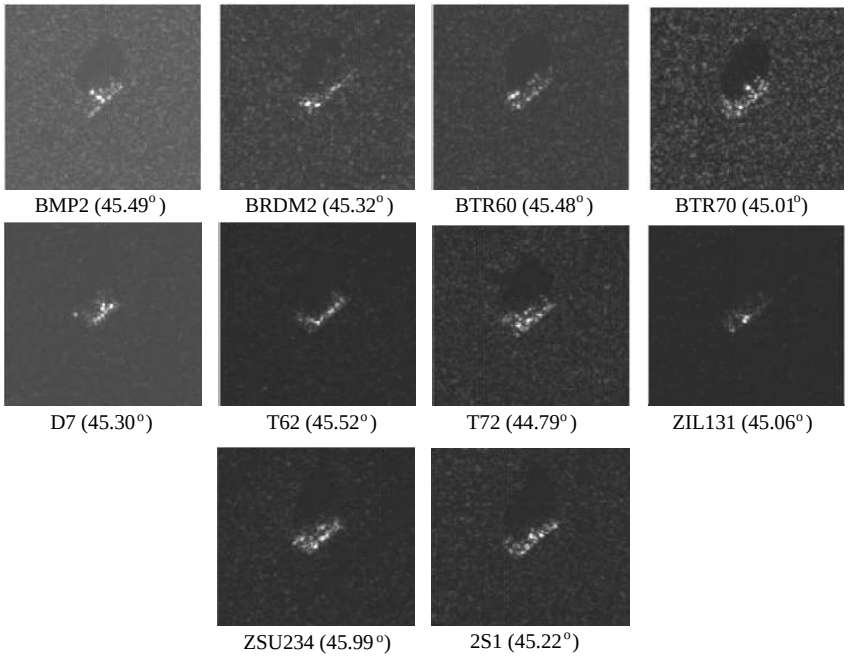

Figure 5. SAR images of ten targets at near aspect angles (the data in brackets are aspect angles).

Table 1. MSTAR Data sets used in classification experiments.

No.	Type	Train (17°)	Test (15°)
1	BMP2	233	196
2	BTR60	256	195
3	BTR70	233	196
4	BRDM2	298	274
5	D7	299	274
6	T62	299	273
7	T72	232	196
8	ZIL131	299	274
9	ZSU234	299	274
10	2S1	299	274

are acquired at 17 degree and 15 degree depression angles over the full 360 degree aspect angles. The data in depression 17 degree are used for training and the other for testing. In MSTAR SAR database, there are 3 different serial numbers for BMP2 and T72. For these two targets, we only use the images from serial number SN_C21 for BMP2 and SN_132 for T72. Table 1 lists the type and sample number of training and testing sets.

The main work before doing classification is the preprocessing of HRR profiles T-F matrices computation and feature vector extraction as described in Section 2 and Section 4. Each T-F matrix was reduced to 25×25 due to the high dimensionality of the original 100×100 T-F matrix.

In the sequel, we will carry out several classification experiments. For comparison, we evaluate the performance of the proposed method on a 10-Class SAR target recognition problem with three features, including NNSC features, NMF features and PCA features. For NMF features extraction, we used the method in [28].

No other additional information was used, e.g., the aspect angle is included in the header of each SAR image chip file. Such information is necessary for template-based classifiers.

5.2. Learning Basis

T-F matrices NNSC feature extraction was obtained for 10, 20, 30, 40, 50, 60, 70, 80, 90, 100, 120, 150 and 200 basis components as described in Section 3. This was done to analyze how the classification results are affected by the number of learning basis. A set of NNSC basis components (computed for all HRR profiles T-F matrices of the training set in the MSTAR database) of dimensionality 20, 50, 100 and 200 is shown in Figure 6. It can be seen that the basis components are both sparse and localized.

5.3. Classification Result

The recognition accuracy obtained by three features extraction techniques with SVM as a function of basis dimension for 10-target classification is shown in Figure 7. For all these experiments, the recognition rates for NNSC, NMF and PCA improve as the basis dimension increases, eventually saturating. However, for NNSC, the rates tend to improve at a faster rate giving higher recognition accuracies for relatively fewer basis dimensions.

From Figure 7, it can be seen that the highest accuracy with NNSC is obtained at a basis dimension of 80. The highest accuracy with NMF is also obtained at a basis dimension of 80. However for PCA, the highest accuracy is obtained at a basis dimension of 200. When NNSC performs best at 80 basis dimensions, the corresponding confusion matrix of 10-target classification results is presented in Table 2. The confusion matrix in Table 3 shows the confusion matrix of 10-target classification best results with NMF at 80 basis dimensions. And the confusion matrix in Table 4 shows the 10-target classification best results with PCA at 200 basis dimensions. The results in Tables 2–4 reveal that SVM classifier achieves an accuracy of 98.78% with NNSC, 92.93% with NMF, and 82.86% with PCA, respectively. It

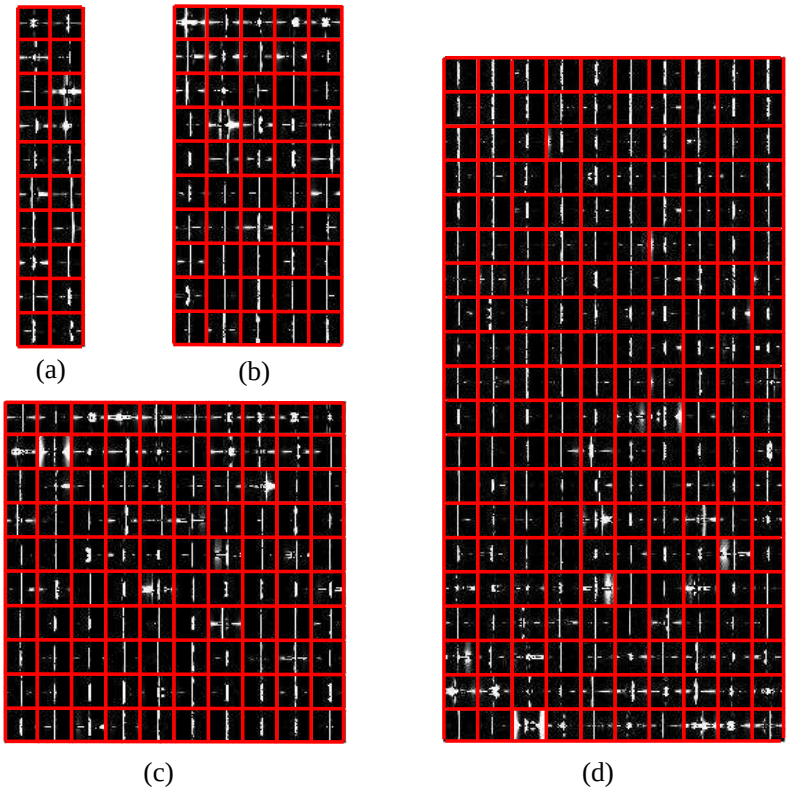

Figure 6. T-F sparse and part-based basis of different dimensions obtained by the NNSC technique. It can be observed that the basis components tend to become more localized as the dimensionality is increased from 20 to 200. (a) 20, (b) 50, (c) 100, (d) 200.

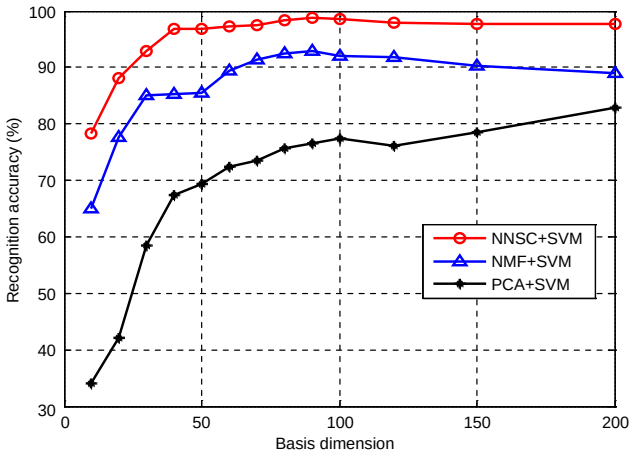

Figure 7. Recognition accuracy vs. basis dimension using three feature extraction methods with SVM for MSTAR 10-target classification.

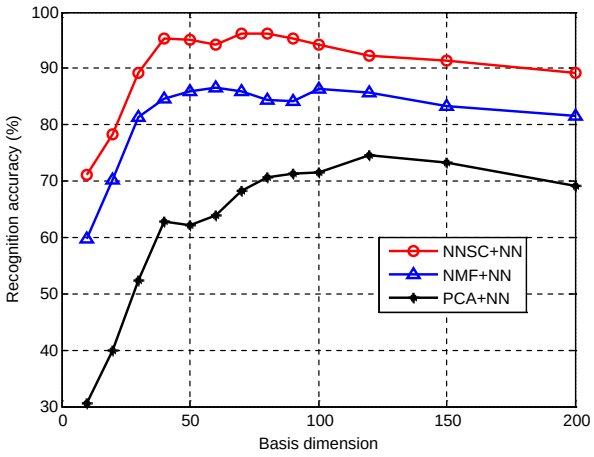

Figure 8. Recognition accuracy vs. basis dimension using three feature extraction methods with NN for MSTAR 10-target classification.

can be seen that NNSC is superior to other methods in the same training and test sets. This confirms the validity and high performance of the proposed approach for SAR ATR. Note that the rates given in Tables 2–4 reflect the "best" recognition rates obtained for the respective technique. They do not indicate which combination of classification algorithm and number of basis dimensions produce this rate.

Table 2. Confusion matrix of 10-target classification results of NNSC + SVM at 80 basis dimensions.

Test	**Train**									
	BMP2 (%)	**BTR60** (%)	**BTR70** (%)	**BRDM2** (%)	**D7** (%)	**T62** (%)	**T72** (%)	**ZIL131** (%)	**ZSU234** (%)	**2S1** (%)
BMP2	**92.35**	0	1.53	0	0	3.57	2.55	0	0	0
BTR60	0	**100**	0	0	0	0	0	0	0	0
BTR70	0	0	**98.47**	1.02	0	0	0.51	0	0	0
BRDM2	0	0	0	**100**	0	0	0	0	0	0
D7	0	0	0	0	**100**	0	0	0	0	0
T62	0	0	0	0	0	**100**	0	0	0	0
T72	0.51	0	0	0	0	0	**96.94**	0	2.55	0
ZIL131	0	0	0	0	0	0	0	**100**	0	0
ZSU234	0	0	0	0	0	0	0	0	**100**	0
2S1	0	0	0	0	0	0	0	0	0	**100**
ACCR (%)	**98.78**									

Note: ACCR means average correct classification rate.

Table 3. Confusion matrix of 10-target classification results of NMF + SVM at 80 basis dimensions.

Test	**Train**									
	BMP2	**BTR60**	**BTR70**	**BRDM2**	**D7**	**T62**	**T72**	**ZIL131**	**ZSU234**	**2S1**
BMP2	**90.82**	2.55	0	0	1.02	0	3.57	0	2.04	0
BTR60	1.54	**83.59**	0.51	3.08	1.03	5.13	1.54	1.03	1.54	1.03
BTR70	1.02	6.12	**79.59**	5.10	0	5.10	0	3.06	0	0
BRDM2	0	0	0	**100**	0	0	0	0	0	0
D7	0	0	0	0	**100**	0	0	0	0	0
T62	2.56	0.37	2.56	0.73	0	**91.58**	0.37	0.37	0.73	0.73
T72	2.55	6.12	1.53	3.57	0	1.02	**83.67**	0	1.53	0
ZIL131	0	0	0	0	0	0	0	**100**	0	0
ZSU234	0	0	0	0	0	0	0	0	**100**	0
2S1	0	0	0	0	0	0	0	0	0	**100**
ACCR (%)	**92.93**									

Figure 8 presents the recognition performance of three feature extraction methods with NN classification algorithm as a function of basis dimension. Tables 5–7 show the best recognition accuracy for different methods with the corresponding basis dimensions. The results in Figure 8 and Tables 5–7 indicate that NNSC obtains the recognition performance superior to the other used methods again when NN algorithm is used. It can be seen that PCA with NN performs the worst. Again, we observe that NNSC performs the best and obtains relative high recognition rates with a low number of basis dimensions. More crucially, NNSC makes about 9.74% improvement over NMF and about 21.7% improvement over PCA.

This implies that PCA cannot deal with T-F matrix localized feature extraction as well as NNSC techniques. From Figure 8, we also observe that recognition performance has significantly declined when basis dimensions are greater than 80 for NNSC. This phenomenon also occurs for the other two methods. This is because NN algorithm is not suitable for high-dimension feature vector classification as SVM. Comparing Figure 7 with Figure 8, it can be seen that the classification performance with SVM is better than that with NN for all kinds of features extraction technique in this paper.

A conclusion can be drawn about PCA and the part-based techniques (including NNSC and NMF) by considering the recognition accuracy. The part-based techniques have a much higher recognition

Table 4. Confusion matrix of 10-target classification results of PCA + SVM at 200 basis dimensions.

Test	Train									
	BMP2	**BTR60**	**BTR70**	**BRDM2**	**D7**	**T62**	**T72**	**ZIL131**	**ZSU234**	**2S1**
BMP2	**70.41**	2.55	5.61	2.55	2.55	4.59	2.04	5.10	4.08	0.51
BTR60	2.56	**83.59**	2.56	0.51	1.54	1.03	3.59	0.51	1.03	3.08
BTR70	2.55	5.61	**78.57**	6.63	0.51	0	3.06	0.51	2.55	0
BRDM2	2.55	1.46	2.19	**85.77**	1.82	0.37	0	3.65	1.09	1.09
D7	2.92	3.65	4.74	4.74	**72.99**	1.82	2.92	2.55	2.19	1.46
T62	1.10	2.93	0.37	2.20	0	**87.18**	0	1.47	2.56	2.20
T72	0.51	3.57	0	2.55	0	0.51	**88.78**	2.55	0.51	1.02
ZIL131	4.74	1.82	2.92	3.65	0.73	0.37	3.28	**80.66**	0.37	1.46
ZSU234	3.28	1.46	0.37	0.37	0	0	1.09	2.19	**89.42**	1.82
2S1	3.28	0	1.09	0	1.82	0	0.37	0	2.19	**91.24**
ACCR (%)	**82.86**									

Table 5. Confusion matrix of 10-target classification results of NNSC + NN at 80 basis dimensions.

Test	Train									
	BMP2 (%)	**BTR60** (%)	**BTR70** (%)	**BRDM2** (%)	**D7** (%)	**T62** (%)	**T72** (%)	**ZIL131** (%)	**ZSU234** (%)	**2S1** (%)
BMP2	**89.29**	0	2.55	1.53	2.04	3.06	0	1.53	0	0
BTR60	0	**100**	0	0	0	0	0	0	0	0
BTR70	0	4.08	**91.84**	2.04	0	0	2.04	0	0	0
BRDM2	0	0	0	**100**	0	0	0	0	0	0
D7	0	0	0	0	**100**	0	0	0	0	0
T62	1.10	2.20	0	0	0	**92.31**	1.83	0	2.56	0
T72	2.55	2.04	3.57	0	0	3.06	**88.78**	0	0	0
ZIL131	0	0	0	0	0	0	0	**100**	0	0
ZSU234	0	0	0	0	0	0	0	0	**100**	0
2S1	0	0	0	0	0	0	0	0	0	**100**
ACCR (%)	**96.22**									

Table 6. Confusion matrix of 10-target classification results of NMF + NN at 100 basis dimensions.

Test	Train									
	BMP2	**BTR60**	**BTR70**	**BRDM2**	**D7**	**T62**	**T72**	**ZIL131**	**ZSU234**	**2S1**
BMP2	**89.80**	3.06	2.55	0	0	1.53	2.55	0	0	0.51
BTR60	1.54	**76.41**	12.82	3.08	1.03	0	1.54	1.03	1.54	1.03
BTR70	0	7.14	**74.49**	0	0	4.08	5.10	4.08	0	5.10
BRDM2	1.82	1.46	2.55	**85.77**	0	2.55	3.65	0	0	2.18
D7	0	0	4.01	0	**86.12**	2.92	2.92	0	2.19	1.82
T62	2.56	0	5.12	1.10	0	**89.02**	0.74	0	0.73	0.73
T72	3.57	6.12	1.53	0	0	1.02	**86.22**	1.53	0	0
ZIL131	3.28	0.73	2.18	0	0	0	2.56	**91.24**	0	0
ZSU234	0	0	0	0	0	0	0	0	**100**	0
2S1	1.82	1.46	0	5.47	0	1.82	1.46	2.19	0	**85.77**
ACCR (%)	**86.48**									

Table 7. Confusion matrix of 10-target classification results of PCA + NN at 120 basis dimensions.

Test	Train									
	BMP2	**BTR60**	**BTR70**	**BRDM2**	**D7**	**T62**	**T72**	**ZIL131**	**ZSU234**	**2S1**
BMP2	**67.86**	2.04	5.61	4.08	2.55	4.59	10.20	0.51	2.04	0.51
BTR60	3.59	**72.82**	1.54	1.54	3.59	11.28	2.56	0.51	1.54	1.03
BTR70	7.65	2.04	**68.37**	5.61	1.02	5.10	2.04	1.53	2.55	4.08
BRDM2	3.28	0.73	1.46	**75.91**	1.82	4.74	6.20	2.19	2.55	1.09
D7	1.82	4.74	3.65	5.84	**72.63**	0.73	3.28	2.19	4.01	1.09
T62	2.56	1.47	1.83	0.73	4.40	**77.29**	5.86	0.73	1.83	3.30
T72	4.08	2.04	1.53	2.55	4.59	2.55	**78.57**	2.55	1.02	0.51
ZIL131	4.38	2.19	3.28	3.28	1.82	6.57	2.19	**70.80**	3.65	1.82
ZSU234	2.92	1.09	0.73	4.01	3.28	1.82	1.09	2.92	**79.56**	2.55
2S1	2.55	3.28	1.09	0.37	1.82	0.73	1.46	5.47	1.82	**81.39**
ACCR (%)	**74.52**									

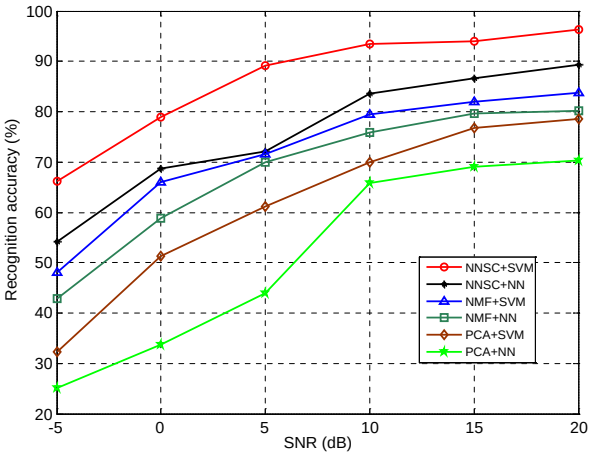

Figure 9. Average correct classification results with different SNR.

correct rate than PCA. This behavior is consistent with the theory that PCA is based on a global transformation of the original space, and the part-based techniques are local in nature. Thus, it turns out that when considering T-F localization, PCA is not able to represent them as well as part-based methods. Clearly, as one would expect, part-based features are superior to holistic features. In part-based methods, from experiment results, it can be seen that NNSC outperforms NMF. Also, it is noted that the high recognition accuracies obtained by NNSC are with a relatively small number of basis dimensions. But this is not the case with NMF.

The obtained recognition accuracy of the proposed method on 10-class SAR ATR tasks is also competitive with previously reported results. In [11], on 10-class SAR ATR tasks they employed HMM classifier with HRR profiles scattering centers features to give the best accuracy of 92.16%, worse than our results. It is worth pointing out that the proposed approach can acquire high recognition accuracy without target poses to be known or estimated. These clearly verify the superiority of the proposed method.

In addition, we consider the effect of random noise to classification performance of the proposed approach. We added Gaussian noise to testing data to evaluate the robustness of each feature extraction algorithm. Figure 9 shows how correct classification rates vary as the signal-to-noise ratio (SNR) varies from -5 dB to 20 dB. From Figure 9, one can identify that NNSC with SVM achieves more than 90% accuracy when SNR is greater than 10 dB, and it decreases rapidly at the SNR levels below 5 dB. But, from the results in Figure 9, it can be seen that NNSC with SVM is superior to the other methods in the whole SNR range.

6. CONCLUSION

The problem of SAR target classification has been addressed in this paper. We have designed and implemented a classification scheme that is based on learning HRR profile T-F features using NNSC. NNSC is employed since it helps reveal the low dimensional structures of the T-F patterns observed in a high dimensional T-F domain. We note that no other literature source has so far reported SAR target classification results using the NNSC technique. The research objective reported in this paper was to demonstrate how the NNSC technique is able to learn parts of a HRR profile T-F matrix and how it can be used for SAR target classification. We have tested three feature extraction techniques: NNSC, NMF and PCA on MSTAR public database. We have compared three features for 10-target classification problem with SVM and NN, respectively. It was found that NNSC with SVM performs much better than other methods and exhibits a strong robustness to noise. It is noted here that the high recognition accuracies obtained by NNSC are with a relatively small number of basis dimensions. Also, it is worth pointing out that the proposed approach can perform well without requiring the poses to be known. However, the computational cost of the proposed method is larger than other methods due to many iterations in AGR and NNSC, which is a weakness. Fast algorithms and further experimentation will be required to settle this issue.

ACKNOWLEDGMENT

This work is supported by the National Natural Science Foundation of China under Grand No. 61301224. This work is also supported by the Fundamental Research Funds for the Central Universities of China under Grant No. CDJRC11160003 and No. CDJZR12160014 and by the Natural Science Foundation Project of CQ CSTC under Grant No. cstcjjA40018 and No. cstc2012jjA40001.

REFERENCES

1. An, D. X., Z.-M. Zhou, X.-T. Huang, and T. Jin, "A novel imaging approach for high resolution squinted spotlight SAR based on the deramping-based technique and azimuth nlcs principle," *Progress In Electromagnetics Research*, Vol. 123, 485–508, 2012.
2. Chiang, C.-Y., Y.-L. Chang, and K.-S. Chen, "SAR image simulation with application to target recognition," *Progress In Electromagnetics Research*, Vol. 119, 35–57, 2011.
3. Dudgeon, D.-E. and R.-T. Lacoss, "An overview of automatic target recognition," *The Lincoln Laboratory Journal*, Vol. 6, 3–9, 1993.
4. Zhao, Q. and J.-C. Principe, "Support vector machines for SAR automatic target recognition," *IEEE Trans. on Aerospace and Electronic Systems*, Vol. 37, No. 2, 643–654, 2001.
5. Zhao, Q., J. C. Principe, V. L. Brennan, D. Xu, and Z. Wang, "Synthetic aperture radar automatic target recognition with three strategies of learning and representation," *Optical Engineering*, Vol. 39, 1230–1236, 2000.
6. Huan, R.-H. and Y. Pan, "Target recognition for multi-aspect SAR images with fusion strategies," *Progress In Electromagnetics Research*, Vol. 134, 267–288, 2013.
7. Papson, S. and R.-M. Narayanan, "Classification via the shadow region in SAR imagery," *IEEE Trans. on Aerospace and Electronic Systems*, Vol. 48, No. 2, 969–980, 2012.
8. Potter, L.-C. and R.-L. Moses, "Attributed scattering centers for SAR ATR," *IEEE Trans. on Image Processing*, Vol. 6, No. 1, 79–91, 1997.
9. Liao, X.-J., P. Runkle, and L. Carin, "Identification of ground targets from sequential high-range-resolution radar signatures," *IEEE Trans. on Aerospace and Electronic Systems*, Vol. 38, No. 4, 1230–1242, 2002.
10. Wong, S., "High range resolution profiles as motion-invariant features for moving ground targets identification in SAR-based automatic target recognition," *IEEE Trans. on Aerospace and Electronic Systems*, Vol. 45, No. 3, 1017–1039, 2009.
11. Albrecht, T. W. and S. C. Gustafson, "Hidden Markov models for classifying SAR target images,"

Proceedings of SPIE, Algorithms for Synthetic Aperture Radar Imagery XI, Vol. 5427, Orlando, FL, USA, Apr. 2004.

12. Nishimoto, M., X. Liao, and L. Carin, "Target identification from multi-aspect high range-resolution radar signatures using a hidden Markov model," *IEICE Trans. Electronics*, Vol. 87, 1706–1714, 2004.
13. Han, S.-K., H.-T. Kim, S.-H. Park, and K.-T. Kim, "Efficient radar target recognition using a combination of range profile and time-frequency analysis," *Progress In Electromagnetics Research*, Vol. 108, 131–140, 2010.
14. Kim, K. T., I. S. Choi, and H. T. Kim, "Efficient radar target classification using adaptive joint time-frequency processing," *IEEE Trans. on Antennas and Propagation*, Vol. 2, No. 48, 1789–1801, 2000.
15. Thayaparan, T., P. Suresh, S. Qian, K. Venkataramaniah, S. SivaSankaraSai, and K. Sridharan, "Micro-Doppler analysis of a rotating target in synthetic aperture radar," *IET Signal Processing*, Vol. 4, 245–255, 2010.
16. Olshausen, B. A., "Emergence of simple-cell receptive field properties by learning a sparse code for natural images," *Nature*, Vol. 381, 607–609, 1996.
17. Wright, J., A.-Y. Yang, A. Ganesh, S.-S. Sastry, and Y. Ma, "Robust face recognition via sparse representation," *IEEE Trans. on Pattern Analysis and Machine Intelligence*, Vol. 31, No. 2, 210–227, 2009.
18. Zhang, H., N.-M. Nasrabadi, Y. Zhang, and T.-S. Huang, "Multi-view automatic target recognition using joint sparse representation," *IEEE Trans. on Aerospace and Electronic Systems*, Vol. 48, No. 3, 2481–2497, 2012.
19. Liu, H., C. Liu, and Y. Huang, "Adaptive feature extraction using sparse coding for machinery fault diagnosis," *Mechanical Systems and Signal Processing*, Vol. 25, 558–574, 2011.
20. Murray, J. F. and K. Kreutz-Delgado, "Learning sparse overcomplete codes for images," *The Journal of VLSI Signal Processing*, Vol.45, 97–110, 2006.
21. Wang, Y., Q. Song, T. Jin, Y. Shi, and X.-T. Huang, "Sparse time-frequency representation based feature extraction method for landmine discrimination," *Progress In Electromagnetics Research*, Vol. 133, 459–475, 2013.
22. Hoyer, P. O., "Modeling receptive fields with non-negative sparse coding," *Neurocomputing*, Vol. 52, 547–552, 2003.
23. Schmidt, M. N., J. Larsen, and F. T. Hsiao, "Wind noise reduction using non-negative sparse coding," *Proceedings of IEEE Workshop on Machine Learning for Signal Processing*, 431–436, 2007.
24. Tan, C.-P., J.-Y. Koay, K.-S. Lim, H.-T. Ewe, and H.-T. Chuah, "Classification of multi-temporal SAR images for rice crops using combined entropy decomposition and support vector machine technique," *Progress In Electromagnetics Research*, Vol. 71, 19–39, 2007.
25. Zhang, Y., S. Wang, and Z. Dong, "Classification of Alzheimer disease based on structural magnetic resonance imaging by kernel support vector machine decision tree," *Progress In Electromagnetics Research*, Vol. 144, 171–184, 2014.
26. Angiulli, G., D. De Carlo, G. Amendola, E. Arnieri, and S. Costanzo, "Support vector regression machines to evaluate resonant frequency of elliptic substrate integrate waveguide resonators," *Progress In Electromagnetics Research*, Vol. 83, 107–118, 2008.
27. Ross, T. D., S. W. Worrell, V. J. Velten, J. C. Mossing, and M. L. Bryant, "Standard SAR ATR evaluation experiments using the MSTAR public release data set," *Proceedings of SPIE, Algorithms for Synthetic Aperture Radar Imagery V*, Vol. 3370, 566–570, 1998.
28. Guillamet, D., B. Schiele, and J. Vitria, "Analyzing non-negative matrix factorization for image classification," *Proceedings of 16th International Conference on Pattern Recognition*, 116–119, 2002.